Journal of Molecular Catalysis A: Chemical 308 (2009) 96–107

Contents lists available at ScienceDirect

Journal of Molecular Catalysis A: Chemical

journal homepage: www.elsevier.com/locate/molcata

Hydrogen reduction kinetics modeling of a precipitated iron Fischer–Tropsch catalyst

Hong Wang[a,b], Yong Yang[a,*], Bao-Shan Wu[a], Jian Xu[a], Ming-Yue Ding[a,b], Hu-Lin Wang[a,b], Wen-Hao Fan[a], Hong-Wei Xiang[a], Yong-Wang Li[a]

[a] State Key Laboratory of Coal Conversion, Institute of Coal Chemistry, Chinese Academy of Sciences, Taiyuan 030001, People's Republic of China
[b] Graduate School of Chinese Academy of Science, Beijing 100039, People's Republic of China

ARTICLE INFO

Article history:
Received 28 November 2008
Received in revised form 19 March 2009
Accepted 20 March 2009
Available online 31 March 2009

Keywords:
Fischer–Tropsch
Iron catalyst
Reduction kinetics

ABSTRACT

Mechanisms and kinetics for the reduction of a precipitated iron-based Fischer–Tropsch catalyst in H_2 have been investigated using in situ Mössbauer effect spectroscopy (MES) and thermogravimetric (TG) method in the temperature range of 250–350 °C. In situ MES results indicate that the reduction of paramagnetic (PM) α-Fe_2O_3 (70%) and superparamagnetic (spm) Fe^{3+} (30%) in the fresh catalyst proceed via different steps. PM α-Fe_2O_3 is firstly reduced to magnetite and then to metallic iron, while the reduction of spm Fe^{3+} proceeds in three consecutive steps: it is first reduced to magnetite with a significantly rapid rate, then to non-stoichiometric wüstite, and finally to metallic iron. The reduction of PM α-Fe_2O_3 to Fe_3O_4 can be described by a two-dimensional Avrami–Erofe' ev phase change model (formation and growth of nuclei). However, the corresponding overall reduction, which includes the reduction of PM α-Fe_2O_3 and spm Fe^{3+} to Fe_3O_4, can be described by a three-dimensional phase-boundary-controlled reaction model based on the overall extraction ratio of oxygen. The difference between the two models selected for the PM α-Fe_2O_3 reduction and the corresponding overall reduction is attributed to the rapid reduction of spm Fe^{3+} to Fe_3O_4. For the reduction of PM magnetite to α-Fe and its corresponding overall reduction (including the reduction of PM and spm Fe_3O_4 to α-Fe), it is found that both of them follow the Avrami–Erofe' ev phase change model (two-dimensional or three-dimensional). The value of apparent activation energy for the overall reduction has been calculated and compared with the literature data.

1. Introduction

Iron catalyst is widely used in Fischer–Tropsch (FT) synthesis as an industrial catalyst by Sasol for the production of a large portion of motor fuels and valuable products from coal or natural gas-based syngas [1]. It is well known that iron phases in the catalyst are not stable under reaction conditions, which can be reduced, oxidized, or carburized during activation and the following FT reaction processes [2,3]. Many studies on the roles of different iron phases in FT synthesis indicated that the phase transformation during activation and reaction processes greatly influence the activity, selectivity, and stability of the catalysts [4–7]. However, kinetics studies on the phase transformation, which are of fundamental importance for the improvement of the performance of iron-based catalyst for FT synthesis, are unfortunately scarce in the literature.

Generally, investigations on the reduction of iron-based FT catalyst in hydrogen mainly focused on the effect of pretreatment condition on the catalytic FT synthesis performance [6,8–11]. X-ray diffraction (XRD) and Mössbauer effect spectroscopy (MES) were commonly used methods in determining the corresponding phase transformations of the catalysts. Bukur et al. [9] followed the phase transformations of a commercially promoted precipitated iron catalyst reduced in hydrogen under a variety of hydrogen flow rates, temperatures and durations with XRD and MES, from which it was observed that the reduced catalyst consisted of metallic iron and/or superparamagnetic (spm) phases. Shroff et al. [6] studied the microstructure change of a precipitated Fe/Cu/K catalyst after different pretreatments using electron microscopy and XRD, and suggested that hematite was first converted to magnetite, then to metallic iron.

The reduction of iron FT catalyst in H_2 was also mentioned in the study of interaction between promoter or binder/support and iron in the catalyst using temperature-programmed reduction (TPR), MES and XRD. Li et al. [12], Wielers et al. [13], and Jin and Datye [14] studied the effect of Cu promoter on the reduction of iron catalyst in hydrogen. They suggested that Cu promoter can facilitate the reduction of iron catalyst. The promoter of K, studied by Yang et al. [15], was found to inhibit the reduction of iron catalyst. Dlamini et al. [4] and Yang et al. [16] studied the influence of SiO_2 addition on the reduction of iron catalyst in hydrogen and found that the

* Corresponding author. Tel.: +86 351 7560835; fax: +86 351 7560668.
E-mail address: yyong@sxicc.ac.cn (Y. Yang).

1381-1169/$ – see front matter © 2009 Elsevier B.V. All rights reserved.
doi:10.1016/j.molcata.2009.03.030

Table 1
Typical kinetic model for gas–solid reaction.

No.	Kinetics process controlling	Equation
1	1D internal diffusion	$\alpha^2 = kt$
2	2D internal diffusion	$(1-\alpha)\ln(1-\alpha)+\alpha = kt$
3	3D internal diffusion	$1-3(1-\alpha)^{2/3}+2(1-\alpha) = kt$
4	1D phase-boundary-controlled reaction/external diffusion	$\alpha = kt$
5	2D phase-boundary-controlled reaction	$1-(1-\alpha)^{1/2} = kt$
6	3D phase-boundary-controlled reaction	$1-(1-\alpha)^{1/3} = kt$
7	1D formation and growth of nuclei (Avrami–Erofe'ev phase change)	$-\ln(1-\alpha) = kt$
8	2D formation and growth of nuclei (Avrami–Erofe'ev phase change)	$[-\ln(1-\alpha)]^{1/2} = kt$
9	3D formation and growth of nuclei (Avrami–Erofe'ev phase change)	$[-\ln(1-\alpha)]^{1/3} = kt$
10	4D formation and growth of nuclei (Avrami–Erofe'ev phase change)	$[-\ln(1-\alpha)]^{1/4} = kt$

reduction of iron catalyst was restrained by the addition of SiO_2, due to its strong interaction with iron.

Although many studies mentioned the reduction of iron-based FT catalysts and some studies even presented schematic representation of the reduction process [6,17–20], little information about the mechanism, rate-controlling step and apparent activation energy of iron catalyst reduction has been reported.

The reduction of iron oxide in hydrogen is a gas–solid reaction, which has been extensively studied in the steel industry, typically using a thermogravimetric (TG) method. Many kinetic models, deduced from the sphere shrink model or the formation and growth of nuclei model (Johnson–Mehl–Avrami–Erofe' ev model), as listed in Table 1, were employed to study the gas–solid reaction. Pineau et al. [21] investigated the reduction of α-Fe_2O_3 by H_2 in the temperature range of 220–680 °C. They found that the reduction of hematite to magnetite follows the formation and growth of nuclei model or phase-boundary reaction model, respectively, depending on temperature range. They also studied the reduction of magnetite obtained from the reduction of hematite in H_2/H_2O atmosphere at 600 or 1200 °C [22]. The results indicated that wüstite was formed between 390 and 570 °C, with further reduction to iron metal at higher temperatures, the reaction rate of which was controlled by diffusion. Similar studies were carried out by Piotrowski [23,24]. It was also found from the literature that the subsequent reduction to Fe follows the formation and growth of nuclei model. It was found that the mathematical modeling of the experimental data presents the rate-controlling step and apparent activation energy, which is significantly important for the controlling of the phase transformation of iron FT catalyst during activation and reaction progress. Similar study has been performed for the iron synthetic ammonia catalyst [25], but few for the iron FT catalyst.

As mentioned above, the reduction of iron FT catalyst was usually studied using the XRD and MES methods. However, the quantitative study of the XRD is not very satisfactory, while the MES method is usually limited to the study of relatively slow reactions due to time spent on spectra collection. In contrast, the TG analysis can follow the weight changes of the sample in a very fast reaction. However, many detailed information of the phase transformation overlap in the TG analysis for the relatively complex reaction process, which makes it difficult to confirm the phase transformation only by TG results. Hence, the combined use of these techniques may provide more insights on the phase transformation of iron FT catalyst.

In the present study, the in situ MES was used to follow the phase transformation of a precipitated iron FT catalyst (with composition of 100Fe/3K/6SiO_2, by mass) during isothermal reduction in hydrogen; while a thermoanalyzer was chosen to follow the iron phase transformations in comparable reduction conditions with the elimination of the effect of hydrogen flow rate and catalyst particle size. The experimental data obtained from both in situ Mössbauer and TG analysis were then fitted by the gas–solid reaction model, from which the apparent activation energy was calculated.

2. Experimental

2.1. Catalyst preparation

The precursor of the catalyst used in the present study was prepared using a precipitation method, namely a flowing aqueous solution of $Fe(NO_3)_3$ and an NH_4OH solution were mixed at 80 °C. The flow rates of the two solutions were adjusted to keep a constant pH value of 8.0 ± 0.1. The precipitate was washed with de-ionized water, and then filtrated. The filter cake was mixed with a mixture of K_2SiO_3 and silica gel with desired amount. The mixture was reslurried with water and sheared at 3000 rpm for 10 min to ensure complete mixing and uniform distribution of SiO_2 and K^+ in the slurry. The sheared slurry was subsequently spray dried in a QZR-5 spray dryer and calcined at 550 °C for 5 h. The weight composition of the catalyst is 100Fe/3K/6SiO_2.

2.2. In situ MES measurement

The Mössbauer measurements were conducted in an MR-351 constant-acceleration Mössbauer spectrometer (FAST, German) consisted of a velocity transducer and a multichannel analyzer. The radioactive source was 25 mCi of ^{57}Co in a Pd matrix. The spectrometer was equipped with a MBF-1100 Mössbauer furnace cell consisting of a quartz tube and a furnace heater coiled on the outer surface of the tube. A chromel–alumel thermocouple was used to measure the temperature at the site of the sample. The temperature was controlled using a TR-55 temperature controller. The furnace was equipped with two windows at each side. The outer windows consist of mylar foil, while the inner windows are made of 0.15 mm thick aluminum foil. The absorption of the 14.4 keV radiation of ^{57}Co by through these windows is less than 1%. A multi-purpose gas handling system can handle flows of H_2 and Ar at 1 atmosphere through the cell [26]. Both H_2 and Ar were of UHP grade and were passed through a series of purification traps to remove tiny amounts of oxygen, carbonyls, and water, respectively, with a flow of 70 ml/min.

About 40 mg of catalyst was pressed under 10 MPa pressure to form a thin disk with diameter of 13 mm and thickness of 0.25 mm. The catalyst disk, located between plates of boron carbide inside a sample holder, was placed in the quartz tube of the Mössbauer furnace cell. The catalyst disk was isothermally reduced as follows. The temperature of the cell was increased to the desired temperature at 30 °C/min in Ar, and then kept for 30 min to remove moisture in the fresh catalyst. The treatment gas was switched to H_2 and the reduction of the catalyst began. After desired reduction time, the atmosphere was switched back to Ar and the temperature of the cell was decreased to room temperature, at which the Mössbauer spectrum was recorded over 20 h. Then the temperature of the cell was re-increased to the same reduction temperature and the atmosphere was switched to H_2 for the continuous reduction.

The Mössbauer spectra were fitted by least-square regression of a sum of Lorentzian lines to the experimental data. The isomer shift (IS), the quadruple splitting (QS), and magnetic hyperfine field (Hhf), were used in identifying the spectral contribution. All isomer shift values reported in the present study were respect to metallic iron (α-Fe).

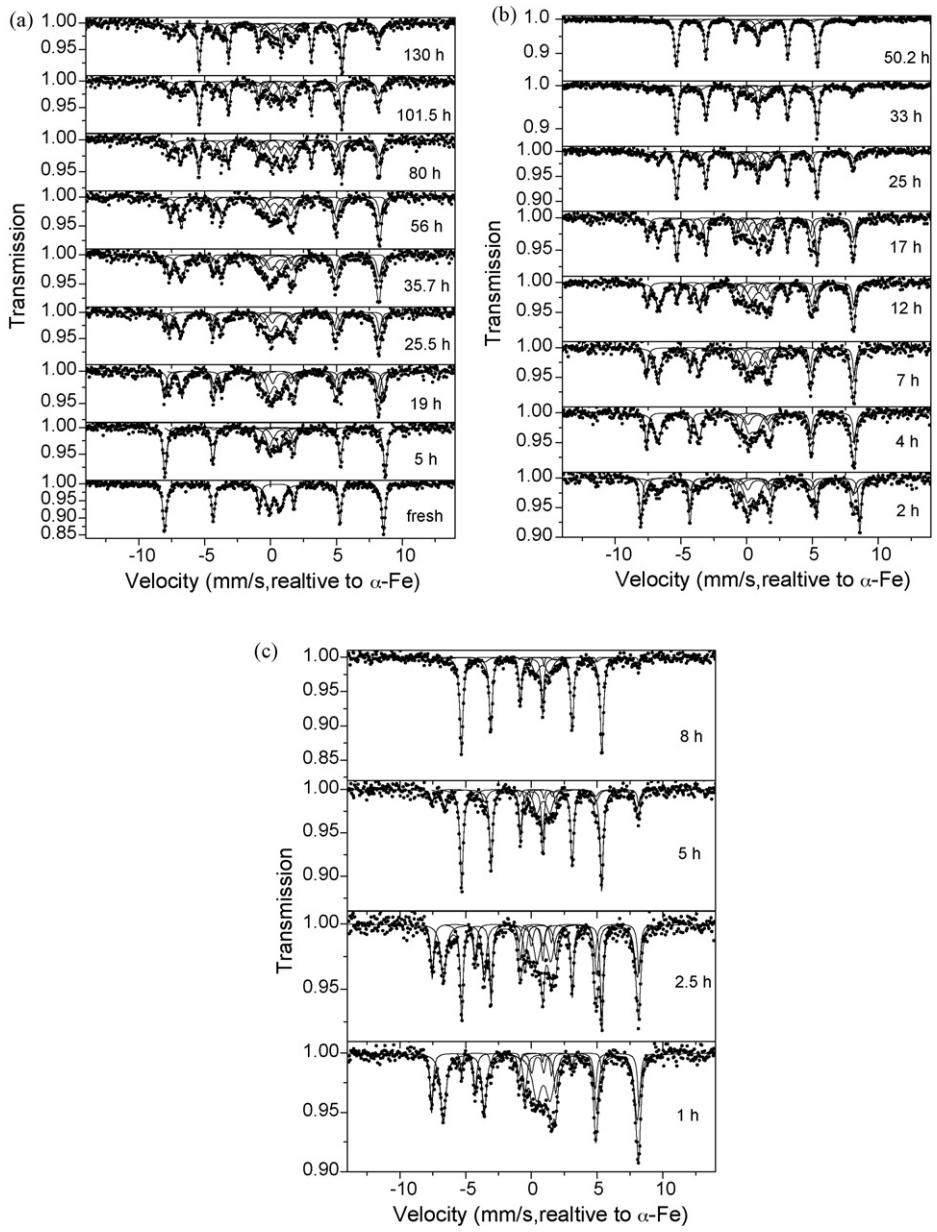

Fig. 1. Mössbauer spectra of catalyst reduced at (a) 250 °C; (b) 300 °C; and (c) 350 °C for various durations.

2.3. Thermogravimetric analysis

Thermogravimetric (TG) analysis was performed in TGA92 (Setaram, France), with a sensibility of 5 μg. 5 mg of catalyst was placed as a single particle layer in an alumina basket hung in the thermobalance. The fresh catalyst was heated in He atmosphere to the desired temperature at a rate of 30 °C/min. The temperature was kept for 30 min to remove moisture in the catalyst. Then He was replaced by H_2 and the weight change of the catalyst was detected as a function of time. Both H_2 and He used in TG analysis were of UHP grade and were purified in a similar procedure to that in the in situ MES measurement.

2.4. Transmission electron microscopy (TEM)

TEM measurements were performed on a JEM 2010 HRTEM (JEOL, Japan) with a point resolution of 2.3 Å. Catalyst was reduced by H_2 in the in situ Mössbauer reactor under conditions as stated in Section 2.2. After desired reduction time, the reactor was switched to Ar atmosphere and decreased to room temperature. Then the sample was passivated with 1% O_2/Ar for 8 h. The passivated samples were crushed and mounted on the grid for the TEM measurements.

3. Results and discussion

3.1. Phase transformation during isothermal reduction

The iron-based FT catalyst was reduced isothermally by hydrogen in the in situ MES cell at 250, 300, and 350 °C, respectively. After various durations on stream, the Mössbauer spectra of the samples were collected at room temperature, which are shown in Fig. 1. Table 2 summarized the average values of Mössbauer parameters associated with iron species in the catalyst during reduction. As shown in Fig. 1a and corresponding Mössbauer parameters in Table 2, the spectrum for the fresh catalyst was fitted with a com-

Table 2
Mössbauer parameters of catalyst during reduction.

Iron phase	IS (mm/s)	ΔE_Q (mm/s)	Hhf (kOe)
α-Fe_2O_3	0.41 ± 0.04	−0.19 ± 0.05	517 ± 3
A-site Fe_3O_4	0.28 ± 0.05	−0.02 ± 0.05	489 ± 3
B-site Fe_3O_4	0.70 ± 0.03	0.01 ± 0.05	459 ± 4
α-Fe	0.02 ± 0.02	0 ± 0.01	334 ± 2
Fe^{3+} in the fresh catalyst	0.31	0.81	–
Fe^{3+}	0.43 ± 0.05	0.86 ± 0.14	–
Fe^{2+}	0.93 ± 0.07	1.23 ± 0.20	–

bination of a sextet and a doublet. The sextet with Hhf of 517 kOe is assigned to the paramagnetic (PM) α-Fe_2O_3 [27] and the doublet is representative of Fe^{3+} in spm state [28]. It is well known that PM α-Fe_2O_3 is hematite with the crystal size larger than 13.5 nm, while spm Fe^{3+} is that with size lower than 13.5 nm [29]. In the present study, the fresh catalyst consists of 70% PM α-Fe_2O_3 and 30% spm Fe^{3+}. As the catalyst reduced in H_2, three additional sextets and a doublet were also detected by Mössbauer spectroscopy. The sextets with Hhf of 489 and 459 kOe can be attributed to tetrahedral (A site) and octahedral sites (B site) of Fe_3O_4, respectively [27]. The sextet with Hhf of 333 kOe is representative of α-Fe in PM state [28]. The doublet with a higher isomer shift (~0.93 mm/s) and quadruple splitting (~1.76 mm/s) is attributed to Fe^{2+} in spm state [11,28]. Raupp and Delgass [30] reported that the critical particle diameter for spm relaxation in α-Fe at room temperature is less than 1.5 nm. In our case, no spm α-Fe was detected during all reduction processes, mainly due to the relative large particle size of α-Fe_2O_3 in the fresh catalyst [11].

The PM phases contents and the overall extraction ratio of oxygen versus time during reduction are given in Fig. 2. The overall extraction ratio of oxygen (α) is calculated based on the in situ MES results and the definition is listed as follow:

$$\alpha = \frac{\sum_i (C_i^0 - C_i^t)V_i}{\sum_i C_i^0 V_i} \quad (1)$$

Where C means the content and V means the valence of iron phases. Subscript (i) indicates the species of iron phases. Superscript means the reduction time. It can be seen from Fig. 2a and b that the reduction of paramagnetic α-Fe_2O_3 involves two stages. Firstly, with the increase of the overall extraction ratio of oxygen up to 0.11, the content of PM α-Fe_2O_3 is decreased from 0.71 to 0, whereas that of PM Fe_3O_4 is increased from 0 to about 0.73, which indicates the reduction of PM α-Fe_2O_3 to PM Fe_3O_4. With the subsequent reduction, the overall extraction ratio of oxygen increases from 0.11. The content of PM Fe_3O_4 decreases gradually, whereas that of PM α-Fe starts to increase, which means that the PM Fe_3O_4 phase is converted to PM α-Fe. The reduction profiles at 350 °C (Fig. 2c) are similar to those at 250 and 300 °C. However, due to the relatively rapid reduction rate and few sampling number at 350 °C, no obvious reduction steps were marked in Fig. 2c. In summary, the isothermal reduction of PM α-Fe_2O_3 in the temperature range of 250–350 °C proceeds in the two following steps:

$$3\alpha\text{-}Fe_2O_3 + H_2 \rightarrow 2Fe_3O_4 + H_2O \quad (2)$$

$$Fe_3O_4 + 4H_2 \rightarrow 3\alpha\text{-}Fe + 4H_2O \quad (3)$$

The content and the mean valence of spm phases during the reduction are also shown in Fig. 2. It can be found that the reduction of the spm Fe^{3+} proceeds in three steps. During the first stage with the overall extraction ratio of oxygen lower than 0.11, the amount of Fe^{3+} is quickly decreased from 0.29 to 0.18, and then remained constant. While the amount of Fe^{2+} is rapidly increased from 0, and then remained 0.08. During the first stage of reduction, the mean valence of the spm phases is quickly decreased to about 2.67, and then remained constant, which is equal to the valence of a standard Fe_3O_4. These results indicate that during the first stage, the α-Fe_2O_3 phase in spm state (namely Fe^{3+}) is reduced to spm Fe_3O_4 (namely $Fe^{3+} + Fe^{2+}$). Moreover, Fig. 2 shows that about 3% of spm phases is converted to PM phases, which may be due to the increase of the particle size resulting from the sintering/agglomeration of the particles during reduction [31], or the lower value of critical particle size of Fe_3O_4 for spm relaxation than that of α-Fe_2O_3 [30]. During the next stage when the overall extraction ratio of oxygen is in the range of 0.11 and 0.20, the content of Fe^{3+} decreased to about 0.07 and that of Fe^{2+} increased to 0.20. The total amount of the spm phases has not obviously changed, and the mean valence is decreased from 2.67 to about 2.25. All of the phenomena indicate that the spm Fe_3O_4 is subsequently reduced to the non-stoichiometric spm wüstite (Fe_xO, $x = 0.89 \pm 0.05$). During the last stage, both the contents of spm Fe^{3+} and spm Fe^{2+} are found to almost remain constant, and the mean valence of the spm phases changes in the range of 2.1–2.4. However, the continuous decrease of the total amount of the spm phases and the increase of PM α-Fe content, indicate that the spm wüstite is converted to PM α-Fe. In summary, the reduction of spm α-Fe_2O_3 proceeds as follows:

$$2\alpha\text{-}Fe_2O_3 + H_2 \rightarrow 3Fe_3O_4 + H_2O \quad (4)$$

$$xFe_3O_4 + (4x-3)H_2 \rightarrow 3Fe_xO + (4x-3)H_2O \quad (x = 0.89 \pm 0.05) \quad (5)$$

$$Fe_xO + H_2 \rightarrow x\alpha\text{-}Fe + H_2O \quad (x = 0.89 \pm 0.05) \quad (6)$$

The reduction behavior of hematite has been investigated extensively. It was suggested that the reduction of hematite by hydrogen proceeds in two or three steps, which mainly depends on the reduction condition employed and the sample used. Pineau et al. [21] studied the reduction of hematite sample, with surface area of 0.51 m^2/g and pore volume of 3.3 cm^3/g, by hydrogen in the temperature range of 220–680 °C. The sample was first reduced to magnetite, and the subsequent reduction of magnetite to iron is a function of the reaction temperature. When the temperature was lower than 420 °C, Fe_3O_4 was reduced directly to iron. In the range of $450 < T < 570$ °C, magnetite and Wüstite were presented together with iron, and at $T > 570$ °C, magnetite is fully reduced to wüstite before its reduction to iron. Typically, the precipitated iron FT catalyst was reduced at temperature lower than 400 °C. Many authors [8,11,12] reported that its reduction proceeds in two steps via magnetite, usually based on the TPR results, which is consistent with the reduction results of PM α-Fe_2O_3 in the present study.

However, Dlamini et al. [4] investigated the effect of SiO_2 addition method on the reduction of iron-based FT catalyst and found that Fe^{2+} species seems to be stable due to the intimate interaction of iron with SiO_2. Wan et al. [32] compared the TPR profiles of the precipitated iron-based FT catalysts with and without SiO_2 addition and believed that wüstite are formed during the reduction of the iron catalyst with SiO_2 addition. Kock et al. [33] also observed the presence of a well-stabilized FeO phase at the temperature where bulk FeO is metastable, and suggested that a temporary stabilization of FeO phase during reduction in H_2 indicated a considerable metal (oxide)-supported interaction. Raupp and Delgass [30] found that the increase of the severity of calcining condition for supported iron catalyst on SiO_2 led to the enhancement of the reducibility of iron oxide. They believed that the increase of the severity of calcining condition resulted in the increase of the particle size and the decrease of the interaction between SiO_2 and iron. In the present study, due to the lower amount of SiO_2 addition in

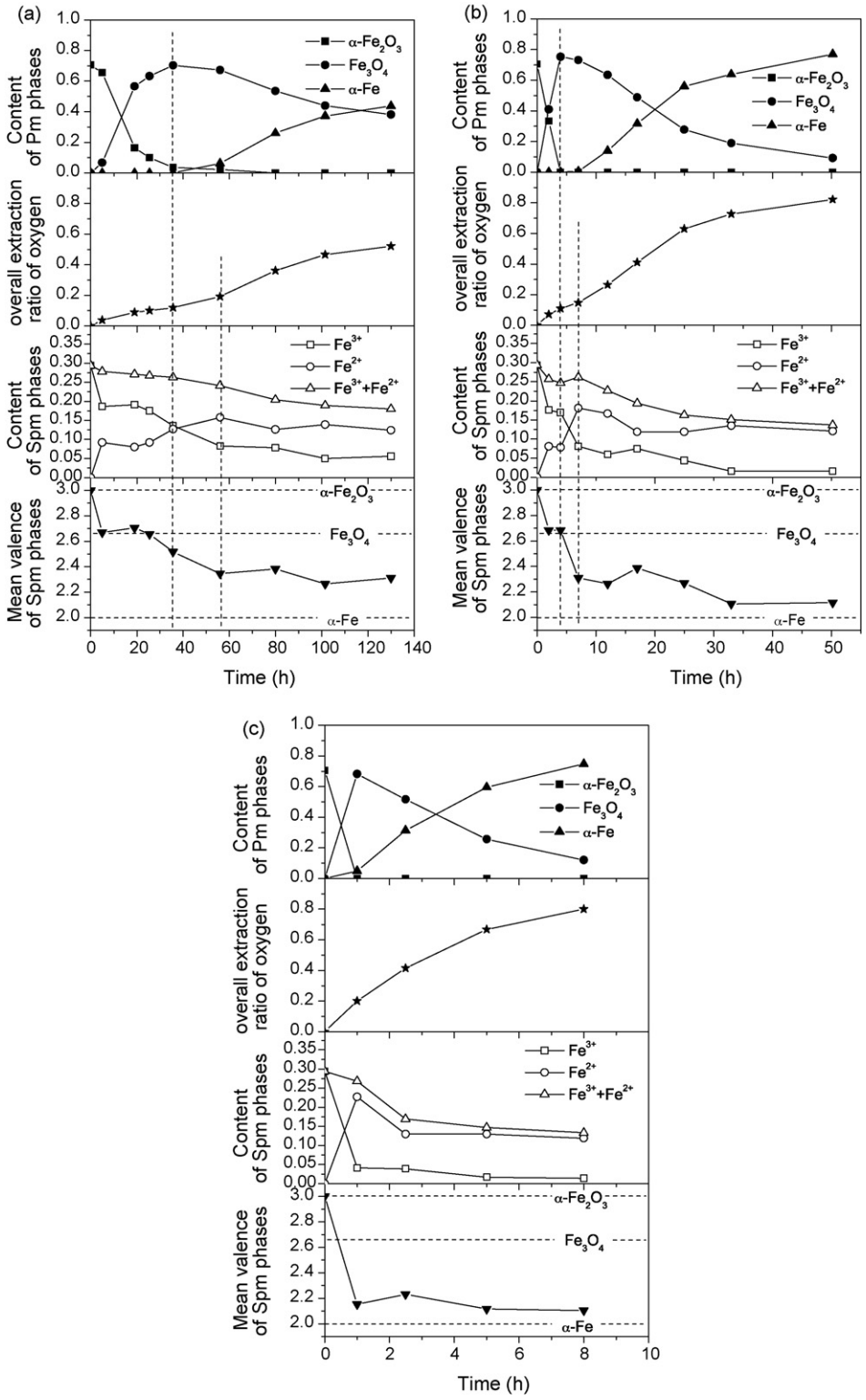

Fig. 2. Changes of PM phase content, overall extraction ratio of oxygen, spm phase content and mean valence of spm phases versus time during reduction in an in situ MES reactor at (a) 250 °C; (b) 300 °C; and (c) 350 °C.

the catalyst (100Fe/6SiO_2, in mass), only a small fraction of iron is contacted with SiO_2 intimately. The addition of SiO_2 enhances the dispersion of iron atom and results in the presence of spm Fe^{3+} in fresh catalyst. The strong interaction of SiO_2 with spm Fe^{3+} leads to the presence of non-stoichiometric wüstite during reduction in H_2 at the temperature where wüstite is metastable. Another interest phenomenon is that the reduction rate of α-Fe_2O_3 to Fe_3O_4 is significantly larger for the spm phases than that for the PM phase. This is quite different with the literature, in which it is reported that the addition of SiO_2 would hinder the reduction of iron oxide [4,14]. However, the results in the literature were obtained based on the comparison of the different catalysts. In the present study the comparison is performed between the hematite with different crystal size in one catalyst. The larger reaction interface and shorter

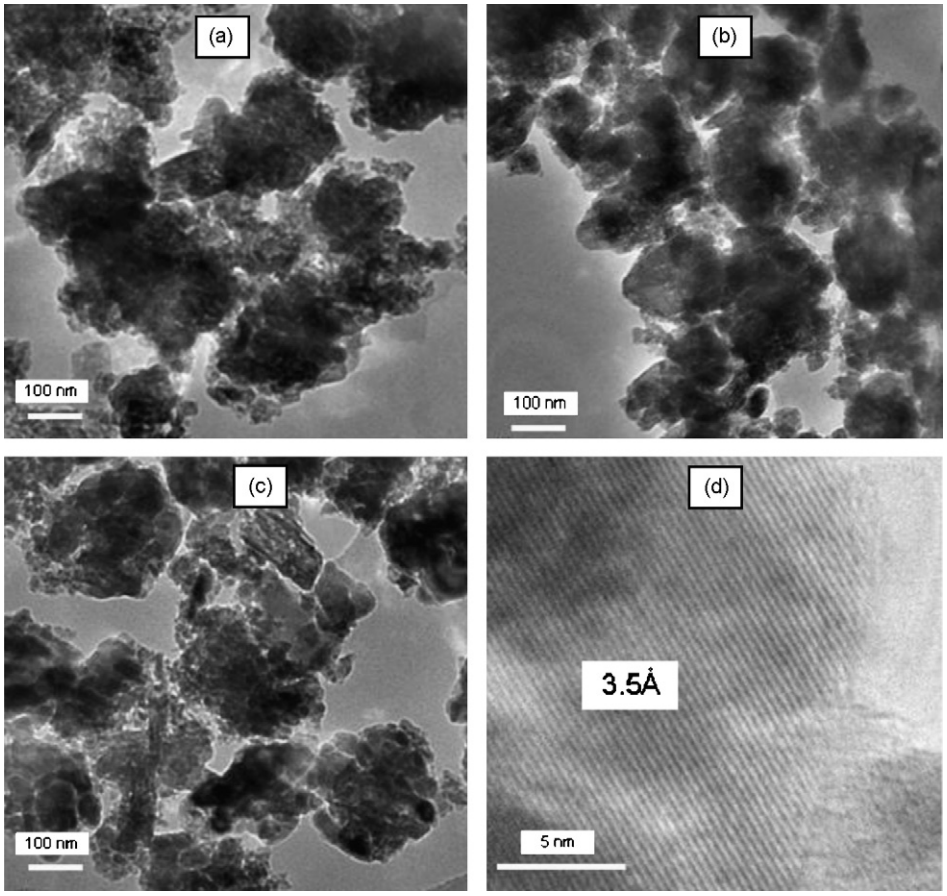

Fig. 3. TEM images of iron-based catalyst during reduction in H_2 at 300 °C for: (a) 0 h; (b) 4 h; and (c) 51 h; and (d) high magnification view of sample (a).

diffusion distance of water result in the more rapid reduction rate of spm hematite than that of PM hematite.

3.2. Kinetic model of the phase transformation in MES experiments

The morphology change of the iron-based FT catalyst during isothermal reduction by hydrogen at 300 °C is shown in Fig. 3. MES characterization indicates that the phase compositions of the passivated samples for TEM measurement are equal to that of the corresponding un-passivated samples. Fig. 3 shows that the fresh catalyst is composed of grains with diameter of about 100 nm. The high magnification view of the fresh catalyst (Fig. 3f) indicates the grain is composed of Fe_2O_3 crystals [6]. During the isothermal reduction, the diameter of the grains almost kept constant and no obvious agglomeration or cracking occurred. The gas–solid reaction models listed in Table 1 are deduced on the basis of the hypothesis that the structure of the sample keeps constant during reaction. The results of Fig. 3 indicate that the reduction process of iron catalyst is suitable to be regressed with the gas–solid models.

In this section, both the conversion (or formation ratio) of each PM phase and the overall extraction ratio of oxygen versus time at relatively low temperature are modeled. The content of spm phases was not modeled due to the rapid reduction rate during the

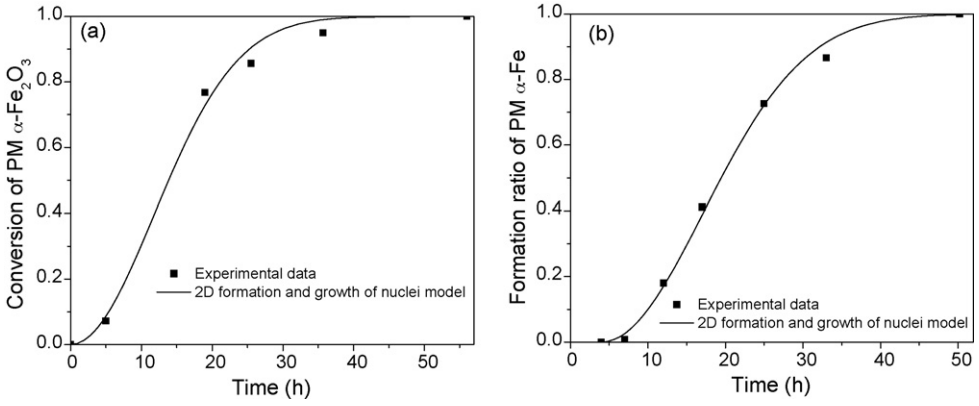

Fig. 4. Mathematical modeling of the content change of PM phases versus time during reduction in an in situ MES reactor: (a) conversion of PM hematite during the first reduction step at 250 °C and (b) formation ratio of PM metallic iron during the second reduction step at 300 °C.

Table 3
Models selection for the content change of PM phases during reduction in an in situ MES reactor.

Process	Model	k (h^{-1})	R^2	No. of data
Conversion of α-Fe_2O_3 during the first reduction step at 250 °C	2D formation and growth of nuclei	0.060	0.994	6
	3D formation and growth of nuclei	0.058	0.985	6
	3D phase-boundary-controlled reaction	0.018	0.967	6
	3D internal diffusion	0.018	0.985	6
	External diffusion	0.023	0.721	6
Formation ratio of Fe_3O_4 during the first reduction step at 250 °C	2D formation and growth of nuclei	0.059	0.990	5
	3D formation and growth of nuclei	0.056	0.971	5
	3D phase-boundary-controlled reaction	0.017	0.968	5
	3D internal diffusion	0.017	0.969	5
	External diffusion	0.030	0.922	5
Conversion of Fe_3O_4 during the second reduction step at 300 °C	2D formation and growth of nuclei	0.053	0.996	7
	3D formation and growth of nuclei	0.055	0.959	7
	3D phase-boundary-controlled reaction	0.014	0.964	7
	3D internal diffusion	0.011	0.913	7
	External diffusion	0.025	0.914	7
Formation ratio of α-Fe during the second reduction step at 300 °C	2D formation and growth of nuclei	0.054	0.997	7
	3D formation and growth of nuclei	0.056	0.963	7
	3D phase-boundary-controlled reaction	0.014	0.959	7
	3D internal diffusion	0.020	0.851	7
	External diffusion	0.026	0.906	7

reduction process of hematite to magnetite and the relatively small content change during the subsequent reduction process. However, the difference between the models for the PM phases and that for the overall exaction ratio of oxygen is attributed to the effect of the reduction of spm phases. The model for the in situ MES results is then applied to the thorough understanding of the kinetic model for the TG results.

The profiles of the conversion of α-Fe_2O_3 and the formation ratio of Fe_3O_4 versus reduction time during the first step obtained at 250 °C were selected to be simulated using the models listed in Table 1, while the profiles of the conversion of Fe_3O_4 and the formation ratio of α-Fe versus reduction time obtained at 300 °C were chosen to be modeled for the second step. The reason of selecting experimental data at 300 °C rather than at 250 °C for the modeling of the second step is that the starting time of the second step can be exactly detected at 300 °C. Fig. 4 shows the profiles of the conversion of α-Fe_2O_3 during the first step and the formation ratio of α-Fe during the second step versus time. It can be found that these profiles are sigmoid-shaped and exhibit three regions: incubation, acceleration, and decay, which indicate that the reaction may follow a nucleation mechanism. The Avrami–Erofe' ev phase change model (2D and 3D) was chosen to fit the experimental data. Furthermore, the data were correlated using 3D phase-boundary-controlled reaction model to account for other factors that may have a possible effect on the reduction process. The results from regression are shown in Table 3 and Fig. 4. From comparison of the correlation coefficient (R^2) value, it can be found that all of the plots, including the conversion of α-Fe_2O_3, the formation of Fe_3O_4, the conversion of Fe_3O_4 and the formation of Fe, can be described by the 2D Avrami–Erofe' ev phase change model.

The 2D Avrami–Erofe' ev phase change model indicates the random nuclei formation and one dimensional growth of the formed nuclei. The schematic representation of the reduction of PM α-Fe_2O_3 deduced from the modeling results is shown in Fig. 5. It can be seen from Fig. 5 that the reduction of PM α-Fe_2O_3 is preceded as follow: first, tiny Fe_3O_4 nuclei are formed randomly in the grain boundary and other imperfections of α-Fe_2O_3 crystal and the reduction rate is very slow. With the continuous reduction, the one-dimensional growth of Fe_3O_4 nuclei becomes the rate-controlling step and the reduction rate is accelerated. When the reduction proceeds in the decaying period, the overlap of Fe_3O_4 nuclei occurs frequently and the reduction rate decreases gradually. After α-Fe_2O_3 was completely converted to Fe_3O_4, tiny Fe nuclei are formed randomly in the boundary of Fe_3O_4 grain, and then the reduction rate is controlled successively by the growth and the overlap of α-Fe nuclei.

The plots of the overall extraction ratio of oxygen versus time at 250, 300, and 350 °C are shown in Fig. 2. It can be seen that the shapes of the plots is relatively complex because that three reactions were included in the plots. Considering the higher content of PM phases (70%) in the catalyst than that of the spm phases (30%), the plots of the overall extraction ratio of oxygen versus time was divided into two parts instead of three parts for the independent modeling. The first part is in the range of the overall extraction ratio of oxygen of 0–0.11, which indicates the overall reduction of hematite to magnetite, and the second is in the range of 0.11–1, which corresponds to the overall reduction of magnetite to metallic iron, including the direct conversion and the indirect conversion via wüstite. Similar to the selection of the experimental data for the modeling of the PM phase content change, the overall reduction of hematite to magnetite at 250 °C and the overall reduction of magnetite to metallic iron at 300 °C are selected to be modeled. According to the plot shape and the factor which have a possible effect on the reduction, the Avrami–Erofe' ev phase change model (1D and 2D), the phase-boundary-controlled reaction model (2D and 3D), and the internal diffusion model (3D) were selected to simulate the plot of the overall reduction of hematite to magnetite versus time at 250 °C, and the Avrami–Erofe' ev phase change model (1D, 2D and 3D), the phase-boundary-controlled reaction model (3D) were selected to simulate the plot of the overall reduction of magnetite to metallic iron versus time at 300 °C. It should be

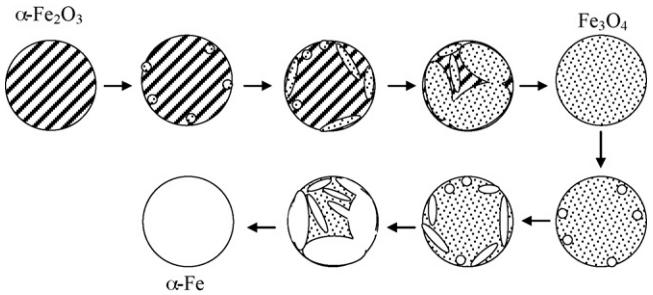

Fig. 5. Schematic representation of the reduction process of PM phases in iron catalyst.

Table 4
Models selection for the overall extraction ratio of oxygen during reduction in an in situ MES reactor.

Process	Model	k (h^{-1})	R^2	No. of data
Overall extraction ratio of oxygen <0.11	1D formation and growth of nuclei	0.088	0.999	4
	2D formation and growth of nuclei	0.128	0.919	4
	2D phase-boundary-controlled reaction	0.030	0.990	4
	3D phase-boundary-controlled reaction	0.023	0.996	4
	3D internal diffusion	0.022	0.969	4
Overall extraction ratio of oxygen >0.11	1D formation and growth of nuclei	0.039	0.860	7
	2D formation and growth of nuclei	0.055	0.994	7
	3D formation and growth of nuclei	0.057	0.949	7
	3D phase-boundary-controlled reaction	0.015	0.975	7

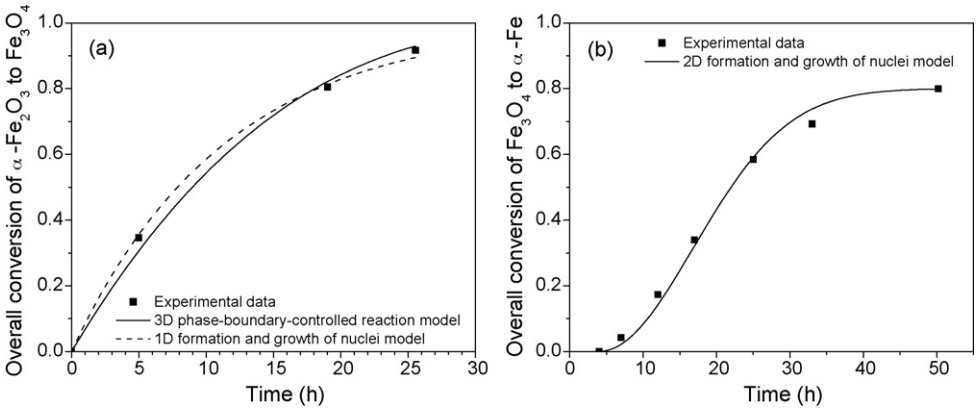

Fig. 6. Mathematical modeling of the overall conversion (including PM and spm phases) versus time during reduction in an in situ MES reactor: (a) overall conversion of hematite to magnetite at 250 °C and (b) overall conversion of magnetite to metallic iron at 300 °C.

noted that the reduction of magnetite to metallic iron cannot be completed even at higher temperature and over prolonged time. The reduction of the remained magnetite is extremely slow. In the present study, the modeling is carried out for the experimental data with the exclusion of the slow reduction of the remainder magnetite. The regression results are shown in Table 4 and Fig. 6. As listed in Table 4, the overall reduction of hematite to magnetite at 250 °C is successfully described both by the Avrami–Erofe' ev phase change model (1D) and by the phase-boundary-controlled reaction model (3D), with the R^2 values higher than 0.995. It has been stated above that the reduction of PM α-Fe_2O_3 to Fe_3O_4 follows the Avrami–Erofe' ev phase change model (2D). The distinction of the model selection for the reduction of PM α-Fe_2O_3 to Fe_3O_4 and that for the corresponding overall reduction is attributed to the rapid reduction of spm Fe^{3+} during the beginning stage of the process, leading to no incubation period present in the plot of the overall reduction of hematite to magnetite versus time. The suitable model is the Avrami–Erofe' ev phase change model (1D) or the phase-boundary-controlled reaction model (3D), rather than the Avrami–Erofe' ev phase change model (2D). For the plot of the overall reduction of magnetite to metallic iron versus time at 300 °C, the most suitable model is the Avrami–Erofe' ev phase change model (2D) according to the R^2 value, which is consistent with the selected model for the reduction of PM Fe_3O_4 to α-Fe.

3.3. Kinetic model of the TG results

The isothermal reduction of the catalyst in hydrogen was also performed using TG method as a complementary method to the in situ MES method. In this section, we first studied both the effect of the hydrogen flow rate and that of the catalyst particle size on the reduction of the catalyst at relatively high temperature (350 °C). Then the isothermal reduction was carried out at 250, 275, 300, 325, and 350 °C with the exclusion of the influences of both the

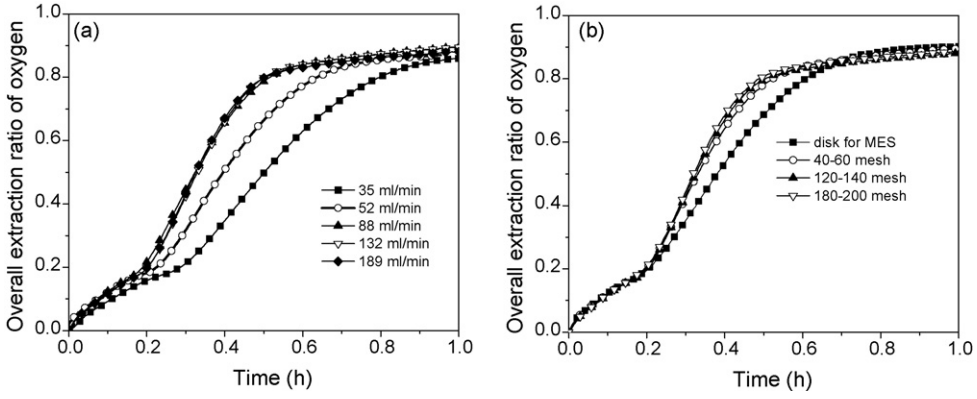

Fig. 7. Effect of: (a) the flow rate of hydrogen and (b) the particle size of catalyst on the reduction of the iron FT catalyst at 350 °C.

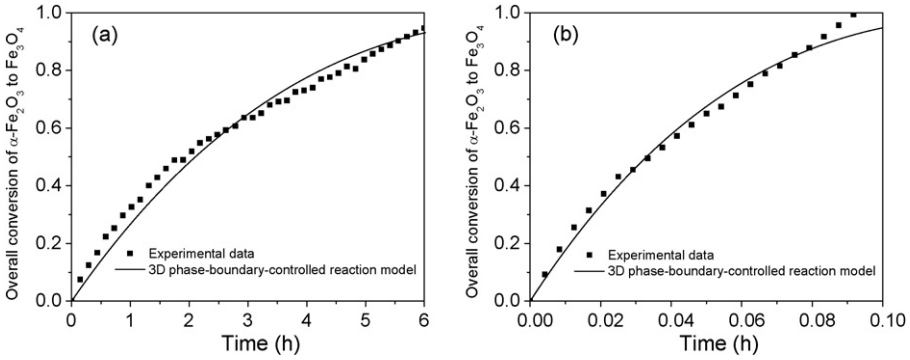

Fig. 8. Mathematical modeling of the overall conversion of hematite to magnetite versus reduction time in a TG analyzer at: (a) 250 °C and (b) 350 °C.

hydrogen flow rate and the catalyst particle size on the reduction. The kinetic model was applied to fit these data. The apparent activation energy was evaluated based on the most suitable kinetic model for the isothermal reduction in the temperature range of 250–350 °C.

Fig. 7 shows the effect of the flow rate of hydrogen and the particle size of catalyst on the reduction at 350 °C. The experiment of the hydrogen flow rate effect on the reduction was performed with the particle size of 120–140 mesh and that of the particle size effect on the reduction was completed with the H_2 flow rate of 189 ml/min. It was found that with the increase of the flow rate of hydrogen, or the decrease of the particle size of the catalyst, the reduction rate is increased obviously. However, when the flow rate was increased above 88 ml/min, the reduction rate is not influenced by the change of the flow rate, indicating the exclusion of the external diffusion control on the reduction. Fig. 7b shows that the effect of internal diffusion on the reduction rate of the catalyst is negligible when the particle size is less than 40–60 mesh. As a result, the isothermal reductions at different temperature were performed with the flow rate of 189 ml/min and the particle size of 120–140 mesh. Furthermore, the results of Fig. 7b also show that the internal diffusion of hydrogen has influenced on the reduction of the catalyst disk for MES results.

Like the in situ Mössbauer results, the isothermal reduction of catalyst in hydrogen in the microbalance reactor is also separated into two processes. The process with the overall extraction ratio of oxygen less than 0.11 is believed as the overall reduction of Fe_2O_3 to Fe_3O_4, and the subsequent process with the overall extraction ratio of oxygen in the range of 0.11–1 is thought as the overall reduction of Fe_3O_4 to α-Fe. The two processes were modeled independently. Fig. 8 shows the profiles of the overall reduction of α-Fe_2O_3 to Fe_3O_4 versus time at 250 and 350 °C. The plots shape of reduction profiles obtained at 275, 300 and 325 °C are similar to that obtained at 250 and 350 °C. According to the plots shape and the regression results for the in situ MES data, the phase-boundary-controlled reaction model (1D, 2D and 3D) and the Avrami–Erofe' ev phase change model (1D) were selected to fit the first reduction process. The regression results are listed in Table 5. The mean deviation (MD) and root mean square deviation (RMSD) are employed for comparison of the models.

Table 5
Models selection for the overall conversion of hematite to magnetite performed in a thermoanalyzer.

Model	T (°C)	k (h^{-1})	MD[a]	RMSD[b]	R^2	No. of data
1D phase-boundary-controlled reaction	250	0.178	0.048	0.108	0.812	1518
	275	0.615	−0.011	0.070	0.854	263
	300	1.752	0.037	0.085	0.898	154
	325	4.632	0.028	0.064	0.944	56
	350	11.888	0.034	0.079	0.921	25
	Sum		0.136	0.406		
2D phase-boundary-controlled reaction	250	0.132	0.011	0.048	0.963	1518
	275	0.446	−0.019	0.028	0.972	263
	300	1.260	0.008	0.032	0.986	154
	325	3.199	0.006	0.027	0.990	56
	350	8.473	0.007	0.031	0.988	25
	Sum		0.014	0.165		
3D phase-boundary-controlled reaction	250	0.098	0.008	0.037	0.978	1518
	275	0.331	0.008	0.034	0.982	263
	300	0.932	0.006	0.027	0.989	154
	325	2.347	0.004	0.029	0.988	56
	350	6.256	0.005	0.030	0.989	25
	Sum		0.031	0.157		
1D formation and growth of nuclei	250	0.363	0.005	0.031	0.985	1518
	275	1.218	0.005	0.035	0.981	263
	300	3.410	0.004	0.038	0.979	154
	325	8.458	0.003	0.045	0.972	56
	350	22.828	0.004	0.043	0.977	25
	Sum		0.021	0.191		

[a] $\mathrm{MD} = \frac{\sum(\alpha_{calc}-\alpha_{exp})}{n}$

[b] $\mathrm{RMSD} = \sqrt{\frac{\sum(\alpha_{calc}-\alpha_{exp})^2}{n-1}}$

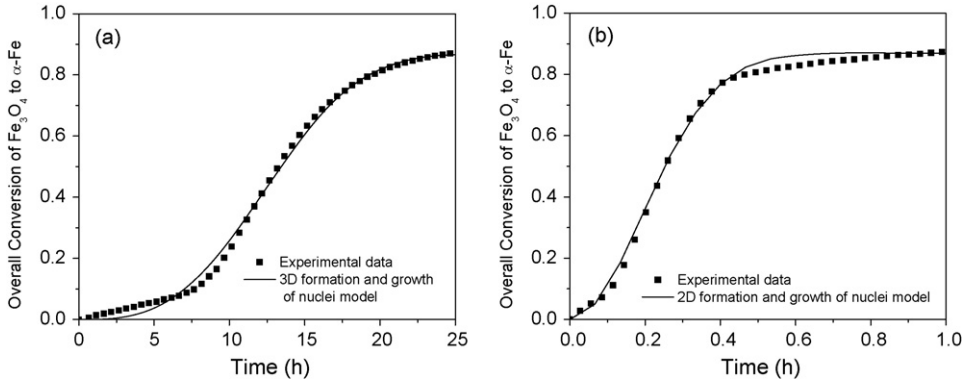

Fig. 9. Mathematical modeling of the overall conversion of magnetite to metallic iron versus reduction time in a TG analyzer at: (a) 250 °C and (b) 350 °C.

From the comparison of the values of MD and RMSD, it can be found that the 3D phase-boundary-controlled reaction model is suitable to describe the overall reduction of α-Fe_2O_3 to Fe_3O_4 in the temperature range of 250–350 °C. The model profiles of the experimental data are also shown in Fig. 8, which confirm the fitting results listed in Table 5. It can be found that the regression results for the TG experimental data are similar to that of the data obtained in the in situ MES experiment at 250 °C. It has been stated that the reduction of PM α-Fe_2O_3 to Fe_3O_4 at 250 °C is controlled by 2D formation and growth of nuclei. However, the rapid reduction of spm Fe^{3+} to Fe_3O_4 results in the suitable model for the plot of the corresponding overall data being the phase-boundary-controlled reaction model (3D), rather than the Avrami–Erofe' ev phase change model (2D). The consistent mechanism for the overall reduction of hematite to magnetite at different temperatures in TG analysis make it reasonable to believe that the reduction of PM hematite to magnetite in the temperature range of 250–350 °C is controlled by the formation and growth of nuclei.

The reduction kinetics of iron oxide was extensively investigated, mainly in the fields of the iron production and the iron catalyst preparation for ammonia synthesis. Pineau et al. [21] studied the reduction of hematite by H_2 in the temperature of 220–680 °C and found that the reaction rate at temperature lower than 420 °C is controlled by two- and three-dimensional growth of nuclei. Piotrowski et al. [23,24] investigated the kinetics of hematite to wüstite and considered magnetite as an intermediate state between Fe_2O_3 and FeO. They reported the Avrami–Erofe' ev phase change model was successfully applied to describe the initial stage of the process. Besides the isothermal reduction experiments, other methods were also employed in studying of the hematite reduction to magnetite. Wimmers et al. [34] studied the reduction mechanism of small Fe_2O_3 particles using temperature-programmed reduction method. The results indicate that the reduction of hematite to magnetite is best described by the three-dimensional Avrami–Erofe' ev phase change model. It can be found that the sample used and temperature employed in the present study is different from that reported in the literature. The hematite used in the present study is prepared using co-precipitated method and with the addition of SiO_2 and K, and reduced at relatively low temperature. The reduction of the main phase in the catalyst (PM hematite) follows the 2D Avrami–Erofe' ev phase change model which is consistent with the literature. However, the greater reduction rate of spm Fe^{3+} than PM α-Fe_2O_3 leads to the overall reduction of hematite being described by the 3D phase-boundary-controlled reaction model, rather than by the 2D Avrami–Erofe' ev phase change model.

Fig. 9 shows the TG profiles for the overall reduction of Fe_3O_4 to α-Fe at 250 and 350 °C. According to the plots shape, the Avrami–Erofe' ev phase change models (2D, 3D and 4D) were selected in fitting the experimental data. The regression results are listed in Table 6. The model profiles of the experimental data are also shown in Fig. 9. It can be found that the overall reduction of Fe_3O_4 to α-Fe process is controlled by the Avrami–Erofe' ev phase change model (2D or 3D), which is consistent both with the regression results for the in situ MES data in the present study and with the literature results [34–36].

Table 6
Models selection for the overall conversion of magnetite to metallic iron performed in a thermoanalyzer.

Model	T (°C)	k (h^{-1})	MD	RMSD	R^2	No. of data
2D formation and growth of nuclei	250	0.070	0.030	0.068	0.963	4215
	275	0.259	0.014	0.044	0.987	729
	300	0.685	0.013	0.041	0.990	462
	325	1.751	−0.001	0.019	0.996	190
	350	3.661	−0.006	0.014	0.992	94
	Sum		0.050	0.186		
3D formation and growth of nuclei	250	0.071	−0.003	0.021	0.997	4215
	275	0.262	−0.011	0.021	0.995	729
	300	0.692	−0.012	0.022	0.995	462
	325	1.792	−0.016	0.044	0.980	190
	350	3.764	−0.016	0.051	0.970	94
	Sum		−0.057	0.159		
4D formation and growth of nuclei	250	0.072	−0.016	0.031	0.991	4215
	275	0.267	−0.016	0.054	0.975	729
	300	0.704	−0.019	0.057	0.979	462
	325	1.832	−0.016	0.082	0.953	190
	350	3.850	−0.016	0.089	0.941	94
	Sum		−0.084	0.312		

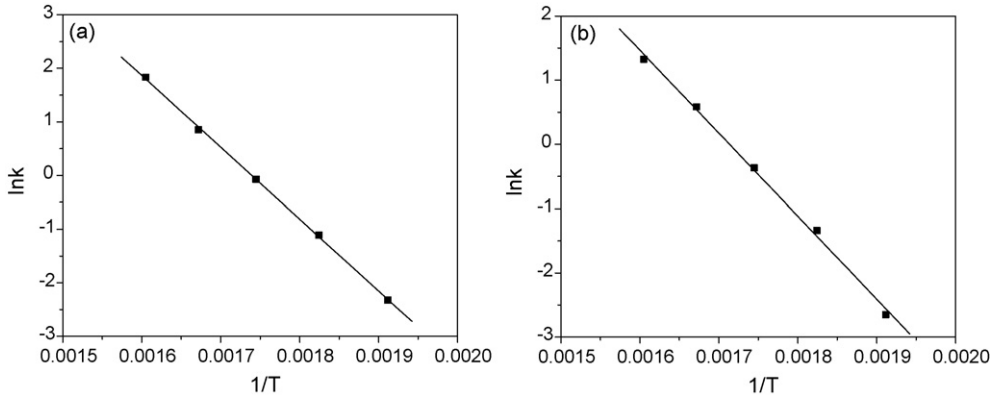

Fig. 10. Arrhenius diagrams for the overall reduction of: (a) hematite to magnetite and (b) magnetite to metallic iron.

Table 7
Summary of apparent activation energy values reported in the literature and comparison with present results.

Source	Process	Temperature range (°C)	Reduction mechanism	ΔE (kJ/mol)
Present	$Fe_2O_3 \rightarrow Fe_3O_4$	250–350	Phase-boundary-controlled reaction (3D)	107
Shimokawabe [37]	$Fe_2O_3 \rightarrow Fe_3O_4$	Linear heating rate	Formation and growth of nuclei (1D)	74–117
Tiernan [35]	$Fe_2O_3 \rightarrow Fe_3O_4$	Linear heating rate	Not determined	106
Tiernan [35]	$Fe_2O_3 \rightarrow Fe_3O_4$	CRTA "rate-jump"	Phase-boundary-controlled reaction	96
Pineau [6]	$Fe_2O_3 \rightarrow Fe_3O_4$	220–680	Phase-boundary-controlled reaction or formation and growth of nuclei	75.9
Present	$Fe_3O_4 \rightarrow Fe$	250–350	Formation and growth of nuclei (3D)	111
Shimokawabe [37]	$Fe_3O_4 \rightarrow Fe$	Linear heating rate	Formation and growth of nuclei (1D)	60–73
Shimokawabe [37]	$Fe_3O_4 \rightarrow Fe$	Linear heating rate	Phase-boundary-controlled reaction	60–73
Tiernan [35]	$Fe_3O_4 \rightarrow Fe$	Linear heating rate	Not determined	54
Tiernan [35]	$Fe_3O_4 \rightarrow Fe$	CRTA "rate-jump"	Formation and growth of nuclei (1D)	59–69
Wimmers [34]	$Fe_3O_4 \rightarrow Fe$	Linear heating rate	Formation and growth of nuclei (1D)	111

It is also found in Table 6 that the reduction at relatively low temperature tends to follow the 3D Avrami–Erofe' ev phase change model and the reduction at relatively high temperature shifts to follow the 2D model. The discrepancy may be due to the slight difference of the activation energy of the formation process and the growth process of nuclei. From the comparison of the sum value of RMSD of every model in Table 6, it is found that the best suitable model for the reduction of Fe_3O_4 to α-Fe in the temperature range of 250–350 °C is the Avrami–Erofe' ev phase change model (3D), which was then used to estimate the apparent activation energy.

Using the reduction rate listed in Tables 5 and 6, the values of the apparent activation energy for both the overall reduction of hematite to magnetite and that of magnetite to metallic iron were calculated based on the Arrhenius equation, which is presented as follow:

$$k = A\exp\left(-\frac{\Delta E}{RT}\right) \quad (7)$$

$$\ln\ k = -\frac{\Delta E}{R}\frac{1}{T} + \ln A \quad (8)$$

The plots of $\ln(k)$ versus $1/T$ are presented in Fig. 10, which exhibit well linear plots, as expected. The slops were then used to estimate the apparent activation energy. A value of 107 kJ/mol was obtained for the overall reduction of hematite to magnetite with correlation coefficient of 0.999, while a value of 111 kJ/mol was calculated for the subsequent overall reduction of magnetite to metallic iron with correlation coefficient of 1.000. Table 7 compares the apparent activation energies obtained in the present study and those reported in the literatures. The present apparent activation energy values for both the overall reduction of hematite to magnetite and that of magnetite to metallic iron are relatively high, but still within the range of results reported in the literature.

4. Conclusions

The reduction of a precipitated iron-based FT catalyst ($100Fe/3K/6SiO_2$ by weight) by hydrogen in the temperature range of 250–350 °C was studied using both an in situ MES and a TG method. The in situ MES results indicate that paramagnetic hematite is first reduced to magnetite, then to metallic Fe; while the reduction of superparamagnetic hematite (namely Fe^{3+}) proceeds in three steps: it is first reduced to magnetite rapidly, then to non-stoichiometric wüstite, and finally to metallic iron.

The mathematical modeling for the in situ MES and TG data suggests that the conversion of PM hematite to magnetic is controlled by the formation and growth of nuclei (2D or 3D). However, due to the rapid conversion of spm Fe^{3+} to magnetite, the plots of the corresponding overall reduction, including the reduction of PM α-Fe_2O_3 and that of spm Fe^{3+}, can be described by the 3D phase-boundary-controlled reaction model. For the reduction of magnetite to metallic iron, both the reduction of PM phase and the corresponding overall reduction can be described by the formation and growth of nuclei model (2D or 3D). Based on the reduction rate in TG experiment, the apparent activation energy was calculated. The value for the overall reduction of hematite to magnetite is about 107 kJ/mol, and that for the overall reduction of magnetite to metallic iron is about 111 kJ/mol.

Acknowledgments

The authors gratefully acknowledge the financial support from Key Program of National Outstanding Young Scientists Foundation of China (20625620) and National Key Basic Research Program of China (2007CB216401). This work is also supported by Synfuels China Co., Ltd.

References

[1] M.E. Dry, Catal. Today 6 (1990) 183.
[2] G. Bian, A. Oonuki, N. Koizumi, H. Nomoto, M. Yamada, J. Mol. Catal. A: Chem. 186 (2002) 203.
[3] N. Sirimanothan, H.H. Hamdeh, Y. Zhang, B.H. Davis, Catal. Lett. 82 (2002) 181.
[4] H. Dlamini, T. Motjope, G. Joorst, G. ter Stege, M. Mdleleni, Catal. Lett. 78 (2002) 201.
[5] J.P. Reymond, P. Mériaudeau, S.J. Teichner, J. Catal. 75 (1982) 39.
[6] M.D. Shroff, D.S. Kalakkad, K.E. Coulter, S.D. Kohler, M.S. Harrington, N.B. Jackson, A.G. Sault, A.K. Datye, J. Catal. 156 (1995) 185.
[7] W.L. van Dijk, H.S. van der Baan, J. Catal. 78 (1982) 24.
[8] D.B. Bukur, L. Nowicki, R.K. Manne, X.S. Lang, J. Catal. 155 (1995) 366.
[9] D.B. Bukur, K. Okabe, M.P. Rosynek, C.P. Li, D.J. Wang, K.R.P.M. Rao, G.P. Huffman, J. Catal. 155 (1995) 353.
[10] C. Huang, B. Ganguly, G.P. Huffman, F.E. Huggins, B.H. Davis, Fuel Sci. Technol. Int. 11 (1993) 1289.
[11] E.S. Lox, G.B. Marin, E. De Grave, P. Bussière, Appl. Catal. 40 (1988) 197.
[12] S. Li, S. Krishnamoorthy, A. Li, G.D. Meitzner, E. Iglesia, J. Catal. 206 (2002) 202.
[13] A.F.H. Wielers, C.E.C.A. Hop, J. van Beijnum, A.M. van der Kraan, J.W. Geus, J. Catal. 121 (1990) 364.
[14] Y. Jin, A.K. Datye, J. Catal. 196 (2000) 8.
[15] Y. Yang, H.W. Xiang, Y.Y. Xu, L. Bai, Y.W. Li, Appl. Catal. A: Gen. 266 (2004) 181.
[16] Y. Yang, H.W. Xiang, L. Tian, H. Wang, C.H. Zhang, Z.C. Tao, Y.Y. Xu, B. Zhong, Y.W. Li, Appl. Catal. A: Gen. 284 (2005) 105.
[17] I.E. Wachs, D.J. Dwyer, E. Iglesia, Appl. Catal. 12 (1984) 201.
[18] S. Li, W. Ding, G.D. Meitzner, E. Iglesia, J. Phys. Chem. B 106 (2002) 85.
[19] K. Nagorny, S. Bubert, J. Catal. 108 (1987) 112.
[20] A.F.H. Wielers, A.J.H.M. Kock, C.E.C.A. Hop, J.W. Geus, A.M. van Der Kraan, J. Catal. 117 (1989) 1.
[21] A. Pineau, N. Kanari, I. Gaballah, Thermochim. Acta 447 (2006) 89.
[22] A. Pineau, N. Kanari, I. Gaballah, Thermochim. Acta 456 (2007) 75.
[23] K. Piotrowski, K. Mondal, H. Lorethova, L. Stonawski, T. Szymanski, T. Wiltowski, Int. J. Hydrogen Energy 30 (2005) 1543.
[24] K. Piotrowski, K. Mondal, T. Wiltowski, P. Dydo, G. Rizeg, Chem. Eng. J. 131 (2007) 73.
[25] A. Barański, A. Bielański, A. Pattek, J. Catal. 26 (1972) 286.
[26] L.M. Tau, S. Borcar, D. Bianchi, C.O. Bennett, J. Catal. 87 (1984) 36.
[27] H.M. Gager, M.C. Hobson, Catal. Rev. 11 (1975) 117.
[28] P.P. Vaishnava, P.I. Ktorides, P.A. Montano, K.J. Mbadcam, G.A. Melson, J. Catal. 96 (1985) 301.
[29] W. Kündig, H. Bömmel, G. Constabaris, R.H. Lindquist, Phys. Rev. 142 (1966) 327.
[30] G.B. Raupp, W.N. Delgass, J. Catal. 58 (1979) 337.
[31] D.B. Bukur, M. Koranne, X. Lang, K.R.P.M. Rao, G.P. Huffman, Appl. Catal. A: Gen. 126 (1995) 85.
[32] H.J. Wan, B.S. Wu, Z.C. Tao, T.Z. Li, X. An, H.W. Xiang, Y.W. Li, J. Mol. Catal. A: Chem. 260 (2006) 255.
[33] A.J.H.M. Kock, H.M. Fortuin, J.W. Geus, J. Catal. 96 (1985) 261.
[34] O.J. Wimmers, P. Arnoldy, J.A. Moulijn, J. Phys. Chem. 90 (1986) 1331.
[35] M.J. Tiernan, P.A. Barnes, G.M.B. Parkes, J. Phys. Chem. B 105 (2001) 220.
[36] S. El-Rahaiby, Y. Rao, Metall. Trans. B 10 (1979) 257.
[37] M. Shimokawabe, R. Furuichi, T. Ishii, Thermochim. Acta 28 (1979) 287.